Hypothalamic neurogenesis persists in the aging brain and is controlled by energy-sensing IGF-I pathway

Zayna Chaker, Caroline George, Marija Petrovska, Jean-Baptiste Caron, Philippe Lacube, Isabelle Caillé, Martin Holzenberger

Hypothalamic neurogenesis persists in the aging brain and is controlled by energy-sensing IGF-I pathway

Abbreviated title

IGF-I and lifelong hypothalamic neurogenesis

Authors

Zayna Chaker [a,b,c,1], Caroline George [a,b], Marija Petrovska [b], Jean-Baptiste Caron [c], Philippe Lacube [a,b], Isabelle Caillé [b,d], Martin Holzenberger [a,b,*]

Affiliations

[a] INSERM, Centre de Recherche UMR938, Hôpital Saint-Antoine, Paris, France

[b] Sorbonne Universités, UPMC – Université Pierre et Marie Curie, Paris, France

[c] Université Paris Descartes, Faculté de Médecine, Paris, France

[d] IBPS, Team Development and Plasticity of Neural Networks, CNRS UMR8246, INSERM U1130, Paris, France

[1] present address: Biozentrum, University of Basel, Basel CH-4056, Switzerland

*Corresponding author

Martin Holzenberger

Inserm UMR938

Faculté de Médecine Pierre et Marie Curie

27 rue Chaligny

F-75012 Paris (France)

Tel +33 (0)140 011 470; Fax +33 (0)140 011 423; martin.holzenberger@inserm.fr

Abstract

Hypothalamic tanycytes are specialized glial cells lining the third ventricle. They were recently identified as adult stem/progenitor cells, able to self-renew and give rise to new neurons postnatally. However, the long-term neurogenic potential of tanycytes and the pathways regulating lifelong cell replacement in the adult hypothalamus are largely unexplored. Using inducible nestin-CreER^{T2} for conditional mutagenesis, we performed lineage tracing of adult hypothalamic stem/progenitor cells (HySC), and demonstrated that new neurons continue to be born throughout adult life. This neurogenesis was targeted to numerous hypothalamic nuclei and produced different types of neurons in the dorsal periventricular regions. Some adult-born neurons integrated the median eminence and arcuate nucleus during aging and produced GHRH. We showed that adult hypothalamic neurogenesis was tightly controlled by insulin-like growth factors (IGF). Knockout of IGF-I receptor from HySC increased neuronal production and enhanced α-tanycyte self-renewal, preserving this stem cell-like population from age-related attrition. Our data indicate that adult hypothalamus retains the capacity of cell renewal, and thus a substantial degree of structural plasticity throughout lifespan.

Keywords

Adult neurogenesis; IGF-I; Hypothalamus; Tanycyte; GHRH; Conditional mutagenesis.

1. Introduction

The hypothalamus is an important structure of the forebrain that integrates and responds to a variety of hormonal and metabolic signals (Williams et al., 2000; Coll and Yeo, 2013). The recent discovery that production of new neurons persists in the postnatal hypothalamus has opened promising lines of research, promoting neurogenesis as potential modulator of adult hypothalamic plasticity and function. However, little is known about the extent and regulation of hypothalamic neurogenesis throughout lifespan, as well as on its possible impact on physiology later in life. Recently, proliferating glial-like cells have been detected lining the paraventricular zone of the adult hypothalamus in rodents (Xu et al., 2005). Although the cell of origin of adult-born hypothalamic neurons is still a matter of debate, α-tanycytes are thought to represent the stem cell-like pool, whereas β-tanycytes, which form a barrier between median eminence (ME) milieu and ventricular cerebrospinal fluid (CSF), show only limited self-renewal (Rodríguez et al., 2005; Robins et al., 2013). In this study, we used conditional mutagenesis driven by a nestin-CreER^{T2} transgene (Lagace et al., 2007) to perform long-term tanycyte lineage tracing *in vivo*. We detected significant production of new neurons in the hypothalamus between 3 and 16 months of age, contributing to cell replacement in various hypothalamic nuclei. Interestingly, several studies suggest that the postnatal dynamics of hypothalamic neurogenesis impacts feeding regulation, but it remains unclear whether increased or decreased neurogenesis is beneficial for long-term energy balance (Lee et al., 2002; Kokoeva et al., 2005; Pierce and Xu, 2010). Conversely, tanycytes are known to respond to a range of trophic factors and energy-sensing pathways (Pérez-Martín et al., 2010), suggesting that environmental changes in diet or activity may influence neurogenesis. Circulating IGF-I is a major molecular integrator of nutrition and exercise acting on adult neurogenesis (Llorens-Martín et al., 2010). Here, we also asked whether somatotropic signaling in adult HySC might be a molecular mechanism coordinating

environmental changes and neurogenesis in the hypothalamic niche. To test this hypothesis, we induced conditional knockout of IGF-I receptor (IGF-1R) specifically in adult nestin^{+} cells, an intervention that mimics food scarcity by genetically lowering cell sensitivity to IGF-I, and quantified short- and long-term effects of this mutation on hypothalamic neurogenesis.

2. Material and methods

2.1. Mouse models

Experimental protocols were approved by *Comité d'éthique pour l'Expérimentation Animale* 'Charles Darwin' (approval N°Ce5/2012/074). All analyses were performed on males. We backcrossed CAG-tdTomato$^{+/0}$ mice (*http://jaxmice.jax.org/strain/007908.html*) to 129/SvPas (129) genetic background. Founder group A was produced crossing CAG-tdTomato$^{+/0}$ with knock-in IGF-1R$^{flox/flox}$ mice on 129 background. Founder group B was obtained crossing nestin-CreER^{T2} transgenic mice with C57BL/6 (B6) background (provided by Dr. Amelia J. Eisch) with IGF-1R$^{flox/flox}$ (B6) mice. The final triple transgenic mutants (nestin-CreER^{T2};CAG-tdTomato$^{+/0}$;IGF-1R$^{flox/flox}$) were generated by crossing founders A and B, resulting in fully reproducible F1 hybrid B6/129 background. In parallel, age-matched control animals were produced on the same F1 hybrid background by crossing nestin-CreER^{T2} (B6) with CAG-TdTomato$^{+/0}$ (129) mice (nestin-CreER^{T2};CAG-TdTomato$^{+/0}$;IGF-1R$^{wt/wt}$). All mice were housed in IVCs under SPF conditions at 21-23 °C, 12 h/12 h light/dark cycle, and food and water *ad libitum*. Control and mutant mice received tamoxifen (Tam; T5648, Sigma-Aldrich) at 12 weeks of age (84 mg kg^{-1} in 2 i.p. injections per day, for 5 consecutive days). Experimental groups of KO and control animals were analyzed 1, 6 and 13 months after induction of Cre recombination.

2.2. Tissue sampling

Mice were anesthetized and perfused transcardially with cold 4% PFA in 0.1 M PBS. Brains were post-fixed overnight at 4°C in 4% PFA, and then incubated in 0.1 M PBS with 30% sucrose until they sank. Brains were snap-frozen in isopentane at -45°C and sectioned into 30 µm slices on a freezing microtome in coronal plane from Bregma -1.22 to -2.54. Coordinates

were determined using a mouse brain atlas (Paxinos and Franklin, 2001). Sections were collected in 6 parallel sets of ten, with sections being 180 µm apart. All 6 sets represented comparable samples of the entire ARC and ME region, and each cell type-specific staining was performed on a given set.

2.3. Immunohistochemistry

Cell type-specific antibody staining was performed on free-floating sections, and combined with Tom^+ newborn cell lineage tracing. Antibodies used were: rabbit polyclonal anti-IGF-1Rβ subunit antibody (sc-713, 1:200, Santa-Cruz Biotechnology), rabbit polyclonal anti-glial fibrillary acidic protein antibody (GFAP, 1:2,000; Dako), anti-nuclear Ki67 antibody (1:250; Millipore), mouse monoclonal anti-neuronal marker antibody (NeuN 1:500; Millipore), rabbit polyclonal anti-P-STAT3 antibody (1:200; Abcam), rabbit polyclonal anti-Neuropeptide Y antibody (1:500; Abcam), mouse monoclonal anti-GABA-B receptor 1 antibody (1:1,000; Abcam), rabbit polyclonal anti-GHRH antibody (1:200; Abcam), and rabbit polyclonal anti-glutamate receptor 1 antibody (AMPA subtype) (1:200; Abcam).

2.4. Cell quantification

All tissues used for quantification were imaged using a spinning disc microscope (Yokogawa spinning head, Roper/Leica). Cell densities and absolute number of neurons were measured on Z-stacks composed of 2 to 4 µm optical slices. Cells were manually counted using Z-stack treatment options of FIJI software (*http://fiji.sc/Fiji*). Tanycytes were identified by their highly specific morphology, and α and β subtypes discriminated based on their anatomical position with respect to the 3rd ventricle (Robins et al., 2013). To assess neuronal morphology, about 20 cells per group were analyzed by acquisition of Z-stacks of 15 to 20

optical sections per neuron at 0.5 µm intervals. 3D-reconstructions of glial cells and neurons were performed using the 3D Project FIJI plug-in.

2.5. Statistical analyses

All data are reported as mean ± SEM. The threshold of statistical significance was defined as $P < 0.05$. Sample size n is the number of mice per experimental group. Student's *t*-test was used to compare groups. $*p < 0.05$, $**p < 0.01$, $***p < 0.001$.

3. Results

3.1. Neuro- and gliogenesis occur beyond postnatal periods in the aging hypothalamic niche

To perform long-term tanycyte lineage tracing, we combine the nestin-CreER^{T2} transgene (Lagace et al., 2007) with Cre-inducible tdTomato knock-in reporter (Madisen et al., 2010). We injected nestin-CreER^{T2};CAG-tdTomato$^{+/0}$ mice with tamoxifen (Tam) at 3 months of age to exclude all developmental neurogenesis (Fig. 1A). Red fluorescence was efficiently induced in ependymocytes (Fig. 1B), and in α- and β-tanycytes (Fig. 1D). This new mouse model allowed cumulative recording of neurogenesis at different time points during adult life and aging. We observed that ependymal cell density increased significantly between 4 and 16 months of age (Fig. 1C; 1,565 ± 387 versus 3,676 ± 476, $p < 0.05$), indicating ongoing proliferation of these support cells in the aging brain. We also demonstrated for the first time a significant age-related attrition of the α-tanycyte compartment (Fig. 1E; -34%, $p = 0.02$). In contrast, β-tanycytes were substantially less abundant than α-tanycytes, and their number remained unchanged with age (Fig. 1F), corroborating the hypothesis that this cell compartment was rather transitory in the adult neurogenic process. Interestingly, the number of Tom^{+}NeuN^{+} cells (Fig. 1G) increased dramatically between 4 and 9 months, reaching a plateau between 9 and 16 months of age (Fig. 1H; 57 ± 3, 237 ± 39 and 196 ± 35 cells, respectively, $p_{4mo\text{-}9mo} = 0.04$). This result clearly demonstrates that production of new neurons continues in the adult hypothalamus. As some postnatal gliogenesis has been reported in this region (Migaud et al., 2010), we quantitatively compared neurogenic and gliogenic fate over age. At 9 and 16 months, we found few newborn cells presenting glial morphology (oligodendrocytes, microglia and astrocytes) in the ventromedial and dorsomedial hypothalamus, as compared to the number of newborn neurons (Fig. 1I-J). Importantly, we

could not detect any gliogenic activity at 4 months, suggesting that limited gliogenesis developed predominantly during late adult life.

3.2. Adult neurogenesis produces specific neuronal cell-types in functionally different regions of the hypothalamus

Adult neurogenesis in the hypothalamic niche was widespread and concerned multiple nuclei located in the posterior (PH), dorsomedial (DMH), ventromedial (VMH), mediobasal and lateral (LH) hypothalamus (Fig. 2A). At 9 months of age, the vast majority of newborn neurons integrated into dorso-medial hypothalamus (PH, DMH and VMH), while the arcuate nucleus (ARC) and median eminence (ME) also received some Tom^+ neurons (Fig. 2A; 49% in PH *versus* 3% in ARC). The long-term integration pattern that we observed differed substantially from the neurogenesis reported from early postnatal periods, confined predominantly to ARC and ME (Lee et al., 2012). Because of this intriguing discrepancy, we aimed at characterizing which types of neuron are born in the aging hypothalamus. We checked whether neurons contributing to the regulation of food satiety were replaced in ARC and VMH, but did not find tangible evidence for colocalization of Tom^+ cells with neuropeptide Y (Fig. 2B; n = 6 animals, > 250 Tom^+ cells screened). Similarly, newborn hypothalamic cells were all negative for P-STAT3, indicating that none of them pertained to the populations of leptin-sensitive, orexigenic neuropeptide Y (NPY/AgRP) or to anorexigenic (proopiomelanocortin, POMC) neurons (Fig. 2C; n = 6, > 250 cells screened). Interestingly, we found that the majority of Tom^+ adult-born cells in the aging ARC-ME were GHRH producing neurons (Fig. 2D; 68% ± 16, n = 6 animals, 25 cells screened in total). In contrast to the situation in the most ventral hypothalamus, DMH and PH contained a substantial proportion of total newborn neurons. These cells were expressing receptors for either glutamate or GABA, the two most abundant neurotransmitters in the hypothalamus

(Fig. 2E-F; 59% were glutamate receptor-positive and 23% GABA receptor-positive, n = 6, > 250 Tom^+ cells screened). This result suggested that adult-born neurons were able to functionally integrate into pre-existing neurocircuitry, possibly as relay interneurons. Although the cell of origin and the differentiation steps of newborn hypothalamic neurons are still a matter of debate, the anatomical disposition of Tom^+NeuN^+ cells around the 3rd ventricle suggested that they were potentially stemming from α-tanycytes and progressively migrated into the hypothalamic parenchyma (Fig. 2G).

3.3. Suppression of IGF-I signaling in adult HySCs delays age-related decline of hypothalamic neurogenesis

To study the role of IGF-I signaling in hypothalamic neurogenesis, we used conditional gene targeting of IGF-1R. Nestin-$CreER^{T2}$;CAG-$tdTomato^{+/0}$;IGF-$1R^{flox/flox}$ mutants and nestin-$CreER^{T2}$;CAG-$tdTomato^{+/0}$ control mice were injected with Tam at 3 months of age to induce HySC-specific IGF-1R knockout. This provoked both red fluorescent label and loss of IGF-1R in all tanycytes and tanycyte progeny in mutants, and red fluorescence in the corresponding cells in control mice, allowing quantitative comparison of IGF-$1R^{-/-}$ and IGF-$1R^{wt/wt}$ newborn cell lineages. We confirmed that tanycytes, ependymocytes, and neurons all express high levels of IGF-1R in wild type animals (Fig. 3A-B). In contrast, adult-born Tom^+ neurons in mutants were completely devoid of IGF-1R (Fig. 3B, right panel).

Using the neuronal marker NeuN, we quantified Tom^+ newborn mature neurons in the hypothalamic niche over age, and observed significantly increased neuronal production in mutants compared to controls at 4 months (Fig. 3C; 158 ± 23 *versus* 57 ± 3, $p_{4mo} = 0.04$), and at 9 months (Fig. 3C; 468 ± 60 *versus* 237 ± 39, $p_{9mo} = 0.008$). Despite noticeable age-related decline of neurogenesis in both groups between 9 and 16 months (-29% in KO *versus* -17% in controls), mutants tended to preserve more adult-born neurons at long-term (Fig. 3C; 331 ± 93

versus 196 ± 35 cells, $p_{16mo} = 0.24$). Of critical note, complete suppression of IGF-I signaling in adult tanycytes did not affect gliogenesis in the aging hypothalamus (9 mo: 48 ± 11 *versus* 57 ± 27, and 16 mo: 28 ± 12 *versus* 31 ± 10, *NS*). Interestingly, the cumulative integration in mutants (Fig. 3D) was similar in proportion to controls (Fig. 2A), confirming that the absolute number of newborn neurons was significantly increased in KO animals in all hypothalamic nuclei, and also along the antero-posterior axis (Fig. 3E). Of important note, most newborn neurons originating from the 3rd ventricle seemed to have migrated long distances before integrating into hypothalamic nuclei in KO and control animals (Fig. 3E). These data clearly demonstrate that deletion of IGF-1R in adult HySC dramatically enhance hypothalamic neurogenesis, both at short and at long-term.

In addition to the impact on neurogenesis, IGF-I signaling also affected the morphology of newborn neuron selectively in the ARC-ME region (Fig. 3F-G). Whether KO or control, adult-born neurons newly integrated into the ARC-ME had significantly smaller soma than those integrated into VMH, DMH and PH (at 16 months of age, KO: 178 ± 28 μm^3 *versus* 522 ± 50 μm^3 and controls: 193 ± 61 μm^3 *versus* 482 ± 81 μm^3; n = 5-7 cells for ARC-ME and n = 18 cells for posterior regions; $p < 0.001$). Interestingly, extensions of IGF-1R$^{-/-}$ nerve cells in the ARC-ME region appeared to be conspicuously more tortuous than in controls at 9 and 16 months of age (Fig. 3G). To quantify tortuosity, we defined dendritic linearity index as curvilinear length divided by the straight line connecting the ends of the measured segment (Irintchev et al., 2005). We found that dendrites of IGF-1R$^{-/-}$ neurons were significantly more tortuous than controls (Fig. 3H; KO: 1.09 ± 0.01 and controls: 1.04 ± 0.01, n = 4-5, $p = 0.04$). Moreover, IGF-1R null neurons also displayed significantly more dendrites sprouting from the soma (Fig. 3G; 4.6 ± 0.5 *versus* 2.0 ± 0.2 dendrites per cell, n = 4-5, $p = 0.012$). These results suggest that outgrowth is strongly dependent on IGF-I signaling also in

the adult brain, and that these effects might be specific to neuroendocrine neurons in arcuate nucleus and median eminence.

3.4. IGF-I signaling controls α-tanycyte maintenance by modulating their division pattern over age

We next asked whether enhanced neurogenesis was accompanied by stem/progenitor cell depletion with age. To address this point, we determined α- and β-tanycyte density in vicinity of the 3rd ventricle. Importantly, at 4 months, KO and controls started with the same number of α-tanycytes (Fig. 4A). In control animals, we observed a marked attrition of this cell compartment in control animals between 4 and 16 months (-48%). In contrast, mutants maintained and even increased the number of α-tanycytes with age (+33%). These differences resulted in twice as many α-tanycytes in mutants compared to controls, both at 9 and 16 months of age (Fig. 4A-B; +132% at 9 months, $p_{9mo} = 0.02$, and +108% at 16 months, $p_{16mo} < 0.0001$). However, we did not observe such age-dependent differences in β-tanycyte density comparing KO and controls (Fig. 4C). Starting with the same number of cells at 4 months, mutants tended to have higher β-tanycyte density at 9 months of age (+78%, $p = 0.24$), but this trend disappeared at age 16 months. Similarly, non-neurogenic ependymal cells seemed unaffected by lifelong suppression of IGF-I signaling (Fig. 4D). Thus, inhibition of IGF signaling in adult HySC prevented age-related depletion selectively in α-tanycytes.

Intriguingly, mutants maintained the pool of α-tanycytes between 9 and 16 months, but produced substantially less neurons at 16 months compared to 9 months. In fact, α-tanycyte density (Fig. 4A) and number of newborn neurons (Fig. 3C) were no longer correlated in the 16-month-old mutants. To explain this discrepancy, we checked whether proliferation propensity decreased in IGF-1R$^{-/-}$ α-tanycytes between 9 and 16 months of age. We found that the proportion of proliferating α-tanycytes was similar at both ages in mutants

(Fig. 4E), indicating that IGF-1R$^{-/-}$ α-tanycytes at 16 months were preferentially self-renewing and less differentiating. This result strongly points to a late-life shift in cell fate choice induced by lifelong suppression of IGF-I signaling in HySC. Collectively, these data demonstrate that deletion of IGF-1R from nestin^{+} cells in the adult hypothalamus allows better maintenance of α-tanycytes specifically with age, possibly through lifelong control of cell division pattern.

4. Discussion

4.1. Neurogenesis in aging versus early-postnatal hypothalamus

Using a conditional genetic marker, we performed long-term lineage tracing of nestin^{+} neuronal progenitors in the hypothalamus. This allowed recording neurogenesis over extended periods of adult life and revealed for the first time quantitative aspects of neuronal replacement in this adult stem cell niche. Published data on SC-dependent maintenance of other adult tissues shows that these processes generally decline with increasing age. Therefore, it is very likely that our findings comprise most if not all of adult neurogenesis after 3 months, and that the bulk of this neurogenesis occurred between 3 and 9 months of age. We demonstrated that hypothalamic neurogenesis generated several types of neurons. Interestingly, identity as well as integration sites of these neurons differed markedly from what has been described for hypothalamic neurons born during postnatal periods. Adult-born neurons mostly integrated into PH, DMH and VMH nuclei, and a smaller proportion was found in the arcuate nucleus and median eminence. Moreover, most of these new neurons were either interneurons receiving GABA and glutamate afferences in posterior hypothalamus, or GHRH neurons in the most ventral regions. We did not find any anorexigenic or orexigenic leptin-sensitive newborn neurons during aging, contrasting with what has been documented for early postnatal hypothalamic neurogenesis (Kokoeva et al., 2005; Rojczyk-Gołębiewska et al., 2014). This intriguing observation suggests that early and late adult neurogenesis of the hypothalamus might contribute to different physiological functions. Several reports show that postnatal neurogenesis in the hypothalamus is controlling energy homeostasis during the first two months of adulthood (Sousa-Ferreira et al., 2014), and accordingly concerns NPY, POMC and P-STAT3 neurons. We propose that the here observed late-life hypothalamic neurogenesis is mainly targeting relay interneurons that might

be important for tuning the activity of specific neuronal circuits in selected nuclei of the hypothalamus.

4.2. Adult-born GHRH-producing neurons

Another surprising observation was that GHRH neurons continued to be produced in the brain throughout adult life. These neurons are important elements in the forward and retro-regulation of the somatotropic neuroendocrine axis. Their nerve endings extend to the median eminence, and GHRH secretion eventually induces growth hormone release from the pituitary into the peripheral blood. It is well-documented that GHRH neurons decrease in number with age (Kuwahara et al., 2004). Thus, *de novo* neurogenesis of specialized neuroendocrine neurons as we demonstrated here may open promising avenues of research for regenerative medicine and novel therapeutic strategies targeting replacement of neuropeptide and hormone-producing cells in the CNS.

4.3. IGF-I signaling, neurogenesis and metabolism

In this study, we demonstrated that hypothalamic neurogenesis continues in the adult and aging brain, which implies that it is controlled by specific molecular pathways throughout lifespan. Previous studies have shown that cell replacement in this new niche is tightly regulated by nutrient-sensing factors, such as brain-derived neurotrophic factor (BDNF), ciliary neurotrophic factor (CNTF) and fibroblast growth factors FGF-2, -10 and -18 (Kokoeva et al., 2005; Robins et al., 2013). Moreover, hypothalamic neurogenesis is known to be highly sensitive to nutritional conditions and metabolic status of the animal. For instance, rodent obesity models display a significant decrease of postnatal neurogenesis in the arcuate nucleus and median eminence (McNay et al., 2012). Inversely, inhibiting hypothalamic neurogenesis is sufficient to alter weight and metabolic balance at short-term

(Lee et al., 2012). Here, we propose that IGF-I signaling, a potent energy-sensing pathway, could serve as a molecular bridge connecting nutrition and cell replacement during adult life and aging. Down-regulation of IGF-I signaling, which is a genetic intervention mimicking conditions of low environmental energy resources, prolongs individual lifespan and preserves regenerative potential of stem cells (Ratajczak et al., 2011). Intriguingly, mutant mice used for the present study also develop a metabolic phenotype at 16 months of age, becoming leaner and more insulin-sensitive with age (Chaker et al., in press). While mostly explained by important changes in olfactory bulb neurogenesis and olfactory sensory function, this phenotype might also be affected by the increased hypothalamic neurogenesis observed at 4 and 9 months of age in mutants. Collectively, our work suggests that the dynamics of neurogenesis in the hypothalamic niche adapts itself to changes in environmental resources and sensory signals. This plasticity seems to be controlled lifelong by IGF signals, and might in turn exert a feed-forward effect on regulation of individual metabolic homeostasis. Interestingly, in mutants and controls, the number of tanycytes far exceeded neurons, raising the issue of whether only a subset of tanycytes has the capacity to generate new neurons. Similarly, as the number of tanycytes was the same in mutants and controls at 4 months, it will be important to parse whether the increase in lineage-traced neurons at all ages in mutant mice stems from increased proliferation rates alone or depends also on increased survival of adult-born neurons.

4.4. IGF signals and α-tanycyte self-renewal during aging

Deletion of IGF-1R shifted the α-tanycyte division pattern towards more self-renewal at long-term, with no effect on β-tanycyte or ependymal cell number. This selective action on the α-tanycyte subset is concordant with IGF-I having more dramatic effects on neurogenesis occurring in the medial periventricular region of the niche, as demonstrated at short-term in 8-

week-old rats (Pérez-Martín et al., 2010). One pending question is whether the cellular mechanism by which IGF-I signaling controls neurogenesis in the hypothalamus is cell autonomous or not. Indeed, ependymocytes, which are an important component of the hypothalamic niche, are also knockout for IGF-1R. This could be sufficient to modify neurogenesis independently of direct effects on stem/progenitor cells, as demonstrated for other genes in subependymal cells of the SVZ (Lim et al., 2000).

5. Conclusions

This work constitutes first proof that highly specific neurogenesis exists in the aging hypothalamus, and that its dynamics depend on the IGF-I pathway. The discovery of lifelong cellular plasticity provides novel insights and perspectives for neuroendocrinology and for the development of hormone replacement therapies.

Acknowledgments

We thank Dr. A.J. Eisch for providing the nestin-CreER^{T2} mouse. This work was funded by INSERM, UPMC and LECMA. Fellowships were provided by AXA Research Fund and FRM.

Author contributions

Z.C., M.H. and I.C. designed research; Z.C., M.P., J.B.C. and P.L. performed experiments; Z.C., M.P., J.B.C., P.L. and I.C. analyzed the data. Z.C. and M.H. wrote the paper. All authors commented on the manuscript.

Disclosure statement

The authors declare they have no conflict of interests.

References

Chaker Z, Aïd S, Berry H, Holzenberger M. Suppression of IGF-I signals in neural stem cells enhances neurogenesis and olfactory function during aging. Aging Cell 2015; in press.

Coll A, Yeo G. The hypothalamus and metabolism : integrating signals to control energy and glucose homeostasis. Curr Opin Pharmacol 2013;13:970–976

Irintchev A, Rollenhagen A, Troncoso E, Kiss ZJ, Schachner M. Structural and functional aberrations in the cerebral cortex of tenascin-C deficient mice. Cerebral Cortex 2005;15:950-962

Kokoeva MV, Yin H, Flier JS. Neurogenesis in the hypothalamus of adult mice: potential role in energy balance. Science 2005;310:679–683

Kuwahara S, Sari DK, Tsukamoto Y, Tanaka S, Sasaki F. Age-related changes in growth hormone (GH) cells in the pituitary gland of male mice are mediated by GH-releasing hormone but not by somatostatin in the hypothalamus. Brain Res 2004;998:164–173

Lagace DC, Whitman MC, Noonan MA, Ables JL, DeCarolis NA, Arguello AA, Donovan MH, Fischer SJ, Farnbauch LA, Beech RD, DiLeone RJ, Greer CA, Mandyam CD, Eisch AJ. Dynamic contribution of nestin-expressing stem cells to adult neurogenesis. J Neurosci 2007;27:12623–12629

Lee DA, Bedont JL, Pak T, Wang H, Song J, Miranda-Angulo A, Takiar V, Charubhumi V, Balordi F, Takebayashi H, Aja S, Ford E, Fishell G, Blackshaw S. Tanycytes of the hypothalamic median eminence form a diet-responsive neurogenic niche. Nat Neurosci 2012;15:700–702

Lee J, Duan W, Mattson MP. Evidence that brain-derived neurotrophic factor is required for basal neurogenesis and mediates, in part, the enhancement of neurogenesis by dietary restriction in the hippocampus of adult mice. J Neurochem 2002;82:1367–1375

Lim DA, Tramontin AD, Trevejo JM, Herrera DG, Garcia-Verdugo JM, Alvarez-Buylla A. Noggin antagonizes BMP signaling to create a niche for adult neurogenesis. Neuron 2000;28:713-726

Llorens-Martín M, Torres-Alemán I, Trejo JL. Exercise modulates insulin-like growth factor 1-dependent and -independent effects on adult hippocampal neurogenesis and behaviour. Mol Cell Neurosci 2010;44:109–117

Madisen L, Zwingman TA, Sunkin SM, Oh SW, Zariwala HA, Gu H, Ng LL, Palmiter RD, Hawrylycz MJ, Jones AR, Lein ES, Zeng H. A robust and high-throughput Cre reporting and characterization system for the whole mouse brain. Nat Neurosci 2010;13:133–140

McNay D, Briançon N, Kokoeva MV, Maratos-Flier E, Flier JS. Remodeling of the arcuate nucleus energy-balance circuit is inhibited in obese mice. J Clin Invest 2012;122:142–152

Migaud M, Batailler M, Segura S, Duittoz A, Franceschini I, Pillon D. Emerging new sites for adult neurogenesis in the mammalian brain: a comparative study between the hypothalamus and the classical neurogenic zones. Eur J Neurosci 2010;32:2042–2052

Paxinos G, Franklin K. The mouse brain in stereotaxic coordinates (2nd edition). San Diego, CA: Academic Press; 2001.

Pérez-Martín M, Cifuentes M, Grondona JM, López-Avalos MD, Gómez-Pinedo U, García-Verdugo JM, Fernández-Llebrez P. IGF-I stimulates neurogenesis in the hypothalamus of adult rats. Eur J Neurosci 2010;31:1533–1548

Pierce AA, Xu AW. De novo neurogenesis in adult hypothalamus as a compensatory mechanism to regulate energy balance. J Neurosci 2010;30:723–730

Ratajczak J, Shin D, Wan W, Liu R, Masternak MM, Piotrowska K, Wiszniewska B, Kucia M, Bartke A, Ratajczak MZ.. Higher number of stem cells in bone marrow of circulating Igf-1 level low Laron dwarf mice - novel view on Igf-1, stem cells and aging. Leukemia 2011;25:729–733

Robins SC, Stewart I, McNay DE, Taylor V, Giachino C, Goetz M, Ninkovic J, Briancon N, Maratos-Flier E, Flier JS, Kokoeva M V, Placzek M. α-Tanycytes of the adult hypothalamic third ventricle include distinct populations of FGF-responsive neural progenitors. Nat Commun 2013;4:2049

Rodríguez EM, Blázquez JL, Pastor FE, Peláez B, Peña P, Peruzzo B, Amat P. Hypothalamic tanycytes: a key component of brain-endocrine interaction. Int Rev Cytol 2005;247:89–164

Rojczyk-Gołębiewska E, Pałasz A, Wiaderkiewicz R. Hypothalamic subependymal niche: a novel site of the adult neurogenesis. Cell Mol Neurobiol 2014;34:631–642

Sousa-Ferreira L, de Almeida LP, Cavadas C. Role of hypothalamic neurogenesis in feeding regulation. Trends Endocrinol Metab 2014;25:80–88

Williams G, Harrold JA, Cutler DJ. The hypothalamus and the regulation of energy homeostasis : lifting the lid on a black box. Proc Nutr Soc 2000;59:385–396

Xu Y, Tamamaki N, Noda T, Kimura K, Itokazu Y, Matsumoto N, Dezawa M, Ide C. Neurogenesis in the ependymal layer of the adult rat 3rd ventricle. Exp Neurol 2005;192:251–264

Figure Legends

Fig. 1. Dynamics of neurogenesis in the aging hypothalamic niche.

(A) Schematics of inducible transgenic approach used for *in vivo* lineage tracing. Administration of Tam activated Cre recombinase in all nestin$^+$ cells, inducing intense red label in these cells and their progeny. All mice were injected at 3 months of age and analyzed 1, 6 and 13 months after Tam-induced labeling. (B) Representative micrograph of recombined ependymal cells (red). Sections were counterstained with DAPI (blue). (C) Age-dependent dynamics of ependymocyte population; $p = 0.05$. (D) Representative micrograph of recombined α- and β-tanyctes (red) lining the 3rd ventricle (3V). Section were counterstained with DAPI (blue). (E and F) Age-dependent dynamics of α-tanycytes (E; $p = 0.02$) and β-tanycytes (F). (G) Sections of dorso-medial hypothalamus stained with neuronal marker NeuN. Arrows indicate adult-born neurons. Scale bars: 50 μm in large micrographs, 10 μm in inset. (H) Age-dependent evolution of neuronal population; $p = 0.04$. (I) Absolute number of Tom$^+$ glial cells detected in the hypothalamic niche at 9 and 16 months. Quantifications were performed on 10 sections per animal and $n_{4mo} = 2$, $n_{9mo} = 6$, $n_{16mo} = 5$ animals per group. (J) 3D Z-projection image representing newborn glial cells (astrocytes co-labeled with GFAP). Scale bar: 10 μm.

Fig. 2. Identity of newborn hypothalamic neurons.

(A) Left panel: Schematic representation of hypothalamic nuclei showing neurogenesis, namely posterior (PH), dorsomedial (DMH), ventromedial (VMH), lateral (LH) and arcuate nucleus (ARC). Right panel: quantification of the proportion of newborn neurons (% of total Tom$^+$ neurons) having integrated into the respective nucleus. (B-F) Double labeling of Tom$^+$ neurons in (B) the ARC-ME region with functional marker NPY and (C) VMH-DMH with P-STAT3 marker, showing no colocalization with Tom$^+$ cells. (D) GHRH staining colocalizing

with a subset of Tom^+ cells in ARC-ME. Scale bars: 50 μm, 200 μm in GHRH inset, 10 μm in merge inset. (E and F) Tissue sections representing DMH nuclei stained using anti-glutamate receptor (E) and anti-GABA receptor (F) antibodies. Scale bars: 10 μm. (G) Representative micrographs of adult-born Tom^+NeuN^+ neurons (arrows) located close to the 3rd ventricle (3V; delimited with dashed lines). Arrangement of these new neurons relative to Tom^+ tanycytes is compatible with the supposed neurogenic role of tanycytes. Depicted events could represent successive stages of adult hypothalamic neurogenesis, with new neurons migrating away from the ventricle walls into the brain parenchyma. Scale bars: 50 μm. All analyses were performed on 9-month-old animals.

Fig. 3. IGF-I signaling and lifelong regulation of hypothalamic neurogenesis.

(A) IGF-1R expression in tanycytes (left) and ependymal cells (right) in the hypothalamic niche. 3rd ventricle (3V) walls are delimited with dashed lines. Arrows indicate $Tom^+IGF\text{-}1R^+$ cells. Scale bars: 10 μm. (B) Tom^+ newborn neurons express IGF-1R in controls (left), while in mutants they do not (right). Scale bars: 50 μm; 10 μm in insets. (C) Number of newborn neurons in the adult hypothalamus over age. n_{4mo} = 2-3 and $n_{9mo\text{-}16mo}$ = 5-6, $p = 0.04$ at 4 months, and $p = 0.008$ at 16 months. (D) Proportion of newborn neurons integrated in each hypothalamic nucleus (% of total Tom^+ neurons in the niche). (E) Neuronal integration map in controls *versus* mutants reported on representative coronal sections of the brain, from Bregma -1.22 to -2.54. The map was built by compiling all Tom^+ cells from 5 animals for each group, using the same number of sections per genotype. (F and G) Representative micrographs of newborn neurons integrated into DMH-VMH-PH (F) and ARC-ME (G) regions of 16-month-old animals. Scale bars: 10 μm. (H) Dendrite morphology of ARC-ME neurons at 16 months of age. Scale bar: 5 μm.

Fig. 4. **IGF-I controls cell fate choice of α-tanycytes throughout lifespan.**

(A-D) Tanycyte and ependymal cell densities in mutant and control mice over age. (A) α-tanycyte density; n = 5-6, $p_{9mo} = 0.017$, $p_{16mo} < 0.0001$. (B) Micrographs illustrating α-tanycyte abundance in KO *versus* control animals. Scale bars: 50 μm. (C) β-tanycyte density. (D) Ependymal cell density. (E) Proportion of proliferating α-tanycytes at 9 and 16 months of age in mutants and controls.

VERIFICATION

1. The authors declare they have no conflict of interests.

2. This work was funded by INSERM, UPMC and LECMA. Fellowships were provided by AXA Research Fund and FRM.

3. The data contained in this manuscript have not been previously published, have not been submitted elsewhere and will not be submitted elsewhere while under consideration at Neurobiology of Aging.

4. Experimental protocols were approved by Comité d'éthique pour l'Expérimentation Animale 'Charles Darwin' (approval N°Ce5/2012/074).

Figure(s)

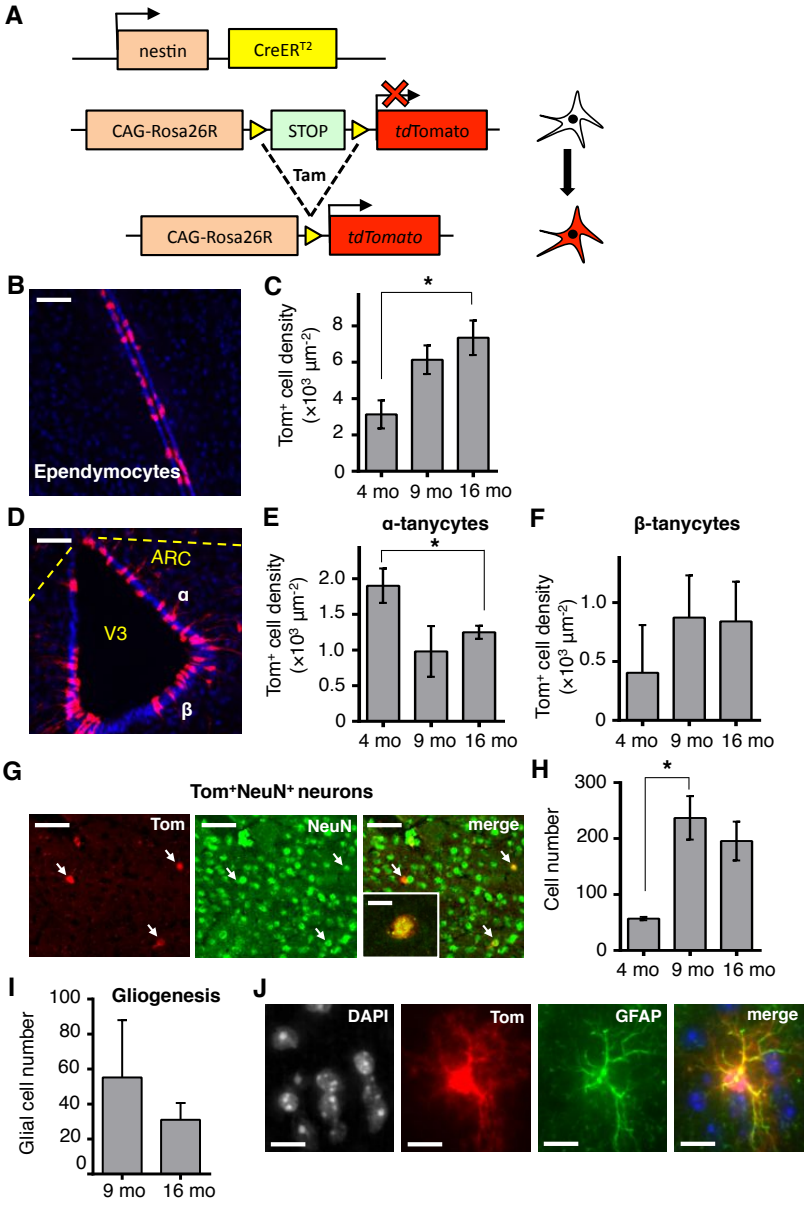

Figure 1 Chaker et al.

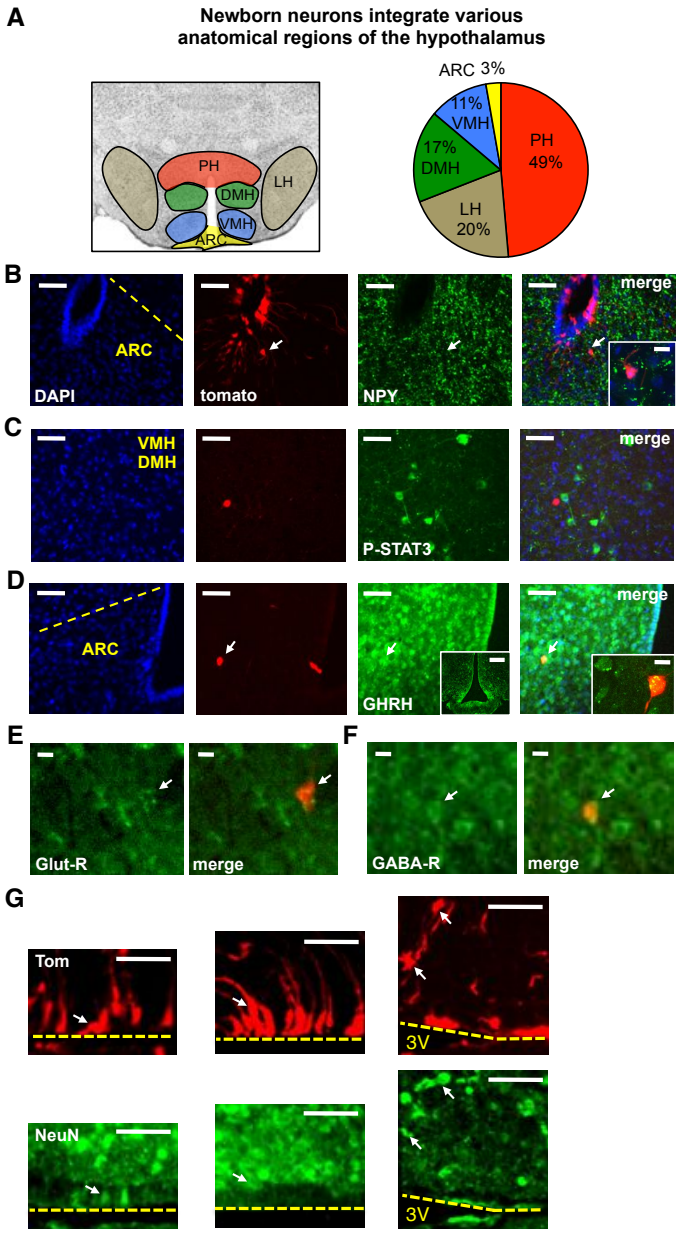

Figure 2 Chaker et al.

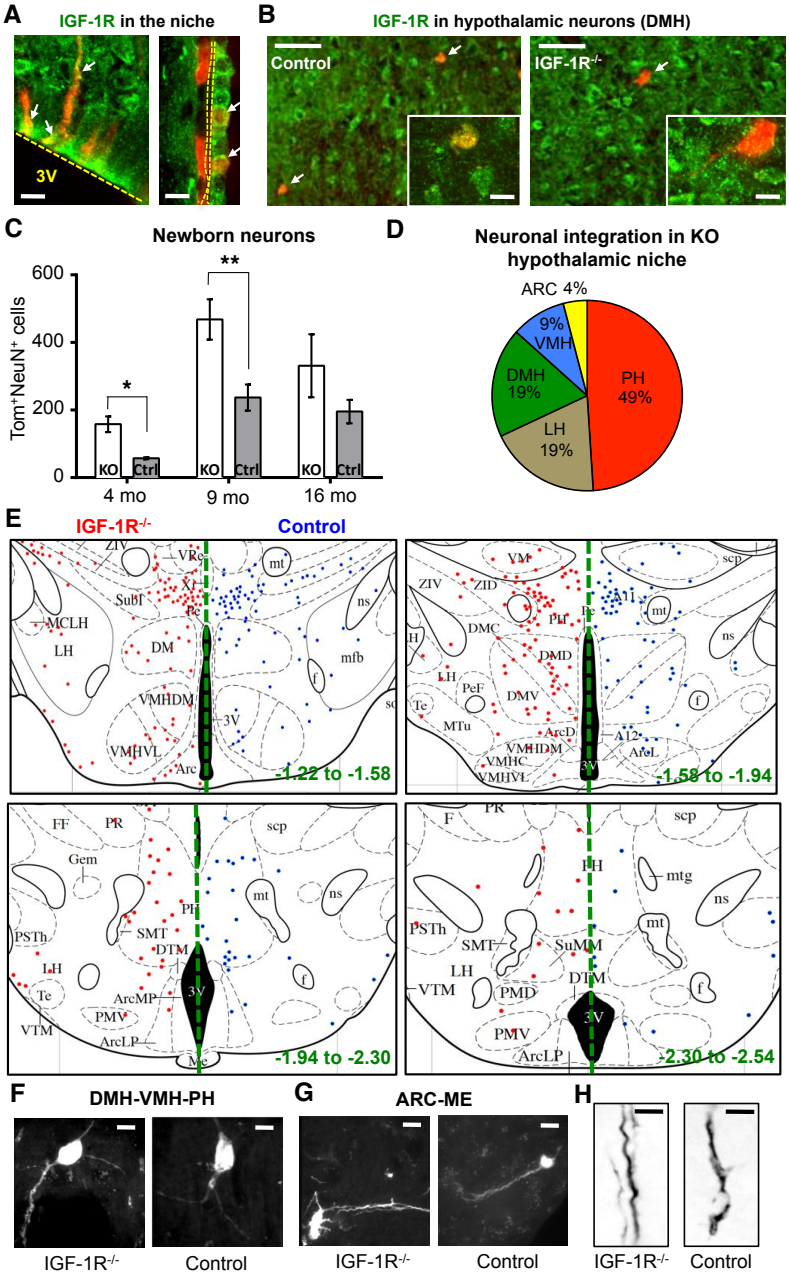

Figure 3

Chaker et al.

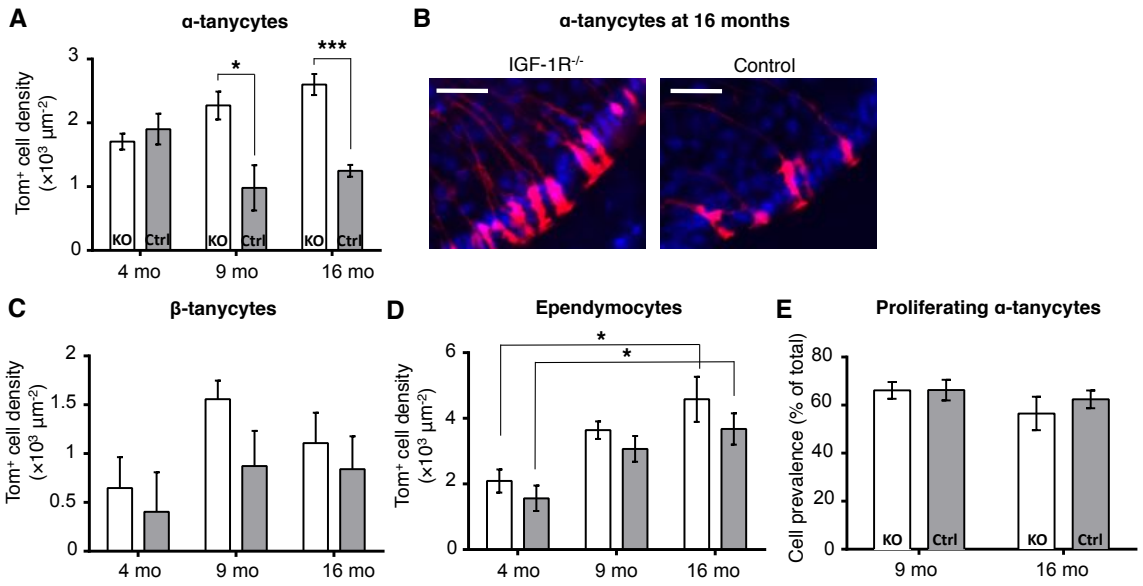

Figure 4 Chaker et al.